Competing Nodal d-Wave Superconductivity and Antiferromagnetism

Xiao Yan Xu and Tarun Grover
Department of Physics, University of California at San Diego, La Jolla, California 92093, USA

(Received 22 September 2020; accepted 7 May 2021; published 27 May 2021)

Competing unconventional superconductivity and antiferromagnetism widely exist in several strongly correlated quantum materials whose direct simulation generally suffers from fermion sign problem. Here, we report unbiased quantum Monte Carlo (QMC) simulations on a sign-problem-free repulsive toy model with same on site symmetries as the standard Hubbard model on a 2D square lattice. Using QMC simulations, supplemented with mean-field and continuum field-theory arguments, we find that it hosts three distinct phases: a nodal d-wave phase, an antiferromagnet, and an intervening phase which hosts coexisting antiferromagnetism and nodeless d-wave superconductivity. The transition from the coexisting phase to the antiferromagnet is described by the $2+1$-D XY universality class, while the one from the coexisting phase to the nodal d-wave phase is described by the Heisenberg-Gross-Neveu theory. The topology of our phase diagram resembles that of layered organic materials which host pressure tuned Mott transition from antiferromagnet to unconventional superconductor at half-filling.

DOI: 10.1103/PhysRevLett.126.217002

Introduction.—The interplay between unconventional superconductivity and magnetism plays a crucial role in a wide variety of strongly correlated systems [1] such as cuprates [2,3], heavy fermions [4–16], layered organic conductors [17–25], iron-based superconductors [26–30], helium-3 [31], and even in recently studied twisted 2D materials [32]. Superconductors with nodal quasiparticles are particularly interesting since the fermionic quasiparticles cannot be neglected even for the ground state properties of the superconductor, or for understanding quantum phase transitions to proximate phases.

One route to obtain an unconventional superconductor is to dope a Mott insulator [3,33], as is experimentally the case for nodal d-wave superconductor (dSC) in cuprates. From a numerical perspective, this is rather challenging: the combination of "Mottness" and continuously varying filling leads to the fermion sign problem, making the unbiased simulation of competing nodal superconductivity and antiferromagnetism an unrealized goal. However, one notes that two of the most prominent symmetry breaking phases in cuprates, namely the dSC or the AFM insulator in principle do *not* require doping for their existence. Therefore, the unbiased large-scale quantum Monte Carlo (QMC) simulations of quantum transitions between dSC and AFM is possible. From an experimental perspective, competing dSC and AFM phases at half-filling are relevant to organic materials [17–25], such as the layered organic material κ-$ET_2Cu[N(CN)_2]Cl$, which undergoes a transition from an AFM Mott insulator to a superconductor under pressure.

In this Letter, we will propose a model which does not suffer from the fermion sign problem, and which demonstrably hosts both a nodal dSC, and an AFM insulator on a 2D square lattice, with an intermediate phase with coexisting AFM and nodeless dSC (denoted as $d\mathrm{SC}_g + \mathrm{AFM}$), through state-of-the-art determinantal QMC (DQMC) simulations. The phase transition between $d\mathrm{SC}_g + \mathrm{AFM}$ and AFM appears to be continuous and in the 3D XY universality class. The phase transition between nodal dSC and $d\mathrm{SC}_g + \mathrm{AFM}$ also appears to be continuous, which we will argue below to lie in the Heisenberg-Gross-Neveu (HGN) universality class.

Model.—The Hilbert space of our model consists of spinful fermions $c_{i,\sigma}$ that live on the vertices $\{i\}$ of a square lattice, and fluctuating cooper pairs $e^{i\theta_{ij}}$ (bosons) living on the bonds $\{ij\}$ of the same square lattice, as shown in Fig. 1(a). The Hamiltonian is given by

$$H = H_t + H_U + H_V + H_{XY}. \tag{1}$$

Here, $H_t + H_U = -t\sum_{\langle ij\rangle,\sigma}(c^\dagger_{i,\sigma}c_{j,\sigma} + \mathrm{H.c.}) + (U/2)\sum_i(\rho_{i,\uparrow} + \rho_{i,\downarrow} - 1)^2$ is the standard Hubbard model with nearest neighbor hopping, with $\rho_{i,\sigma} = c^\dagger_{i,\sigma}c_{i,\sigma}$. H_V is the coupling between fermion operator corresponding to d-wave pairing and rotors θ, $H_V = V\sum_{\langle ij\rangle}[\tau_{i,j}e^{i\theta_{ij}}(c^\dagger_{i,\uparrow}c^\dagger_{j,\downarrow} - c^\dagger_{i,\downarrow}c^\dagger_{j,\uparrow}) + \mathrm{H.c.}]$ with $\tau_{i,i\pm\hat{x}} = 1$, $\tau_{i,i\pm\hat{y}} = -1$. Finally, H_{XY} is a quantum rotor Hamiltonian describing the dynamics and self-interactions of cooper pairs: $H_{XY} = K\sum_{\langle ij\rangle} n^2_{ij} - J\sum_{\langle ij,il\rangle}\cos(\theta_{ij} - \theta_{il})$, where n_{ij} is the angular momentum of rotors, $[n_{ij}, e^{\pm i\theta_{ij}}] = \pm e^{\pm i\theta_{ij}}$, and $\sum_{\langle ij,il\rangle}$ denotes summation over all pairs of nearest neighbor bonds, i.e., bonds that share a site. We note the K term is the kinetic part of the fluctuating cooper pairs, and the J term will be generated

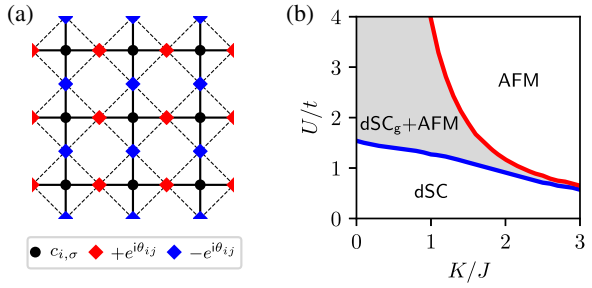

FIG. 1. The lattice model and mean-field phase diagram at $V/t = 0.5$. (a) The lattice model. Fermions (black circle dots) live on a square lattice with nearest hopping and on-site Hubbard interaction U. Rotors (colored square dots) live on the bonds of the same square lattice described by a quantum rotor Hamiltonian. Rotors coupled to fermion pairing operators with the d-wave form indicated by different signs ($\tau_{ij} = \pm 1$) in front of $e^{i\theta_{ij}}$. (b) Mean-field phase diagram. dSC stands for the nodal $d_{x^2-y^2}$ superconductor, AFM for the antiferromagnetic insulator, and $d\mathrm{SC}_g + \mathrm{AFM}$ for the coexisting gapped d-wave superconductor and antiferromagnetic insulator.

dynamically. The model has the same symmetries as the conventional Hubbard model: a spin-rotation SU(2) symmetry and a charge U(1) symmetry given by $c_{i,\sigma} \to c_{i,\sigma} e^{i\varphi}$, $\theta \to \theta + 2\varphi$. It also has a particle-hole symmetry $c_{i,\sigma} \to \epsilon_i c^\dagger_{i,\sigma}$, $\theta \to -\theta$, at half-filling, where $\epsilon_i = (-)^i$. Perhaps most importantly, the model also hosts an anti-unitary symmetry $\mathcal{U}$: $c_{i,\uparrow} \to \epsilon_i c^\dagger_{i,\downarrow}, c_{i,\downarrow} \to -\epsilon_i c^\dagger_{i,\uparrow}, i \to -i$, and $\mathcal{U}^2 = -1$, which makes the model sign problem free [34].

One may obtain some features of the global phase diagram of our model without detailed calculations. Setting $U = 0$, when $K/J \ll 1$, the charge-U(1) symmetry will be spontaneously broken, and therefore, the fermion part of the Hamiltonian reduces to the BCS mean-field theory for a nodal $d_{x^2-y^2}$ superconductor, which we denote as dSC. The dSC phase is expected to be stable at small U since weak interactions are irrelevant for the nodal Dirac fermions. When K/J increases, eventually the charge-U(1) symmetry is expected to get restored due to fluctuations of the θ field. Since the unit cell of H contains an odd number of fermions, a gapped trivial paramagnet is ruled out [35,36], and energetically, we expect the phase at $U/t \gg 1$ and $K/J \gg 1$ to be a conventional antiferromagnet. Furthermore, since the nodes in dSC are separated by (π, π), which is the ordering wave vector for AFM, one may also expect a phase where AFM coexists with a *gapped* d-wave superconductor. As well we see, these expectations are born out by the DQMC calculations, but first, we consider a mean-field theory.

Mean-field phase diagram.—Defining $\hat{\alpha}_{ij} \equiv -e^{i\theta_{ij}}$ and $\hat{\Delta}_{ij} \equiv \tau_{i,j}(c^\dagger_{i,\uparrow} c^\dagger_{j,\downarrow} - c^\dagger_{i,\downarrow} c^\dagger_{j,\uparrow})$, we are led to two coupled mean-field Hamiltonians, one for the fermions, H_f^{MF} and the other for the rotors, H_θ^{MF}: $H_f^{\mathrm{MF}} = -t \sum_{\langle ij\rangle,\sigma} (c^\dagger_{i,\sigma} c_{j,\sigma} + \mathrm{H.c.}) - Um \sum_i (-)^i (\rho_{i,\uparrow} - \rho_{i,\downarrow}) - V\alpha \sum_{\langle ij\rangle} (\hat{\Delta}_{ij} + \mathrm{H.c.})$, and $H_\theta^{\mathrm{MF}} = K \sum_{\langle ij\rangle} n_{ij}^2 - J \sum_{\langle ij,il\rangle} \cos(\theta_{ij} - \theta_{il}) - V\Delta \sum_{\langle ij\rangle} (\hat{\alpha}_{ij} + \mathrm{H.c.})$. Here, $\alpha = \langle \hat{\alpha}_{ij} \rangle$, $\Delta = \langle \hat{\Delta}_{ij} \rangle$, and $m = \langle (-)^i (\rho_{i,\uparrow} - \rho_{i,\downarrow}) \rangle$, and we have chosen the antiferromagnetic order parameter to point along the z axis in the spin space. We can solve the two coupled mean-field Hamiltonians self-consistently. The H_θ^{MF} part is still an interacting rotor lattice problem which we solve using numerical exact diagonalization (ED) on a small cluster consisting of four bonds of a square lattice. After we obtain the value of α, we solve the fermion part H_f^{MF}, and find a self-consistent solution. We set $t = 1$, $J = 1$, $V/t = 0.5$, and explore the U/t-K/J phase diagram as shown in Fig. 1(b). At small U/t, the (nodal) dSC is a stable phase, while at larger U/t, we enter a phase with coexisting gapped d-wave superconductivity ($d\mathrm{SC}_g$) and antiferromagnetism (AFM). At still larger U/t, a pure AFM phase without any superconductivity is stabilized. Tuning K/J changes the relative sizes of these three phases. Overall, when we increase K/J, the pure AFM region becomes larger, while the coexistence phase region ($d\mathrm{SC}_g + \mathrm{AFM}$) shrinks. We note that a variational cluster perturbation theory and cluster dynamical mean-field theory calculations on doped repulsive Hubbard model also find a coexistence phase similar to ours ($d\mathrm{SC}_g + \mathrm{AFM}$) [37–42].

QMC phase diagram.—The model can be simulated with the DQMC method without sign problem (see Refs. [43,47,48] for additional technical details of DQMC). In DQMC, the imaginary time evolution is Trotter decomposed into L_τ slices, $\beta t = L_\tau \Delta_\tau$, where imaginary time step $\Delta_\tau = 0.1$ is used in our simulations. We employ the standard Hubbard-Stratonovich transformation to decouple the repulsive Hubbard interaction into fermion bilinears coupled to auxiliary fields [49]. To explore the ground state properties, we scale the inverse temperature with the linear system size L, in particular, we fix $\beta t = 2L$ and perform simulations up to $L = 20$. Motivated by the mean-field phase diagram in the U/t-K/J plane, one only needs to tune one parameter to explore all three possible phases. We fix parameters $U/t = 4.0$, $V/t = 0.5$, and explore possible phases by tuning only K/J. The AFM order parameter $\vec{m} = \langle (-)^i \vec{S}_i \rangle$, and the dSC order parameter $\alpha = \langle \hat{\alpha}_{ij} \rangle$, are extracted from static correlation functions $m^2 = (1/L^4) \sum_{i,j} (-)^{i+j} \langle \vec{S}_i \cdot \vec{S}_j \rangle$ and $\alpha^2 = (1/4L^4) \sum_{\langle ij\rangle,\langle kl\rangle} \langle e^{i\theta_{ij}} e^{i\theta_{kl}} \rangle$. Figure 2 shows these order parameters extrapolated to the thermodynamic limit, see [43] for technical details. For $K/J < 1.92(5)$, only $\alpha \neq 0$, which corresponds to the nodal dSC phase. This is also evident from the spectral function integrated over a small energy window, Fig. 3(a), which shows four distinct nodes. For $1.92(5) < K/J < 2.40(5)$, we have both $\alpha \neq 0$ and

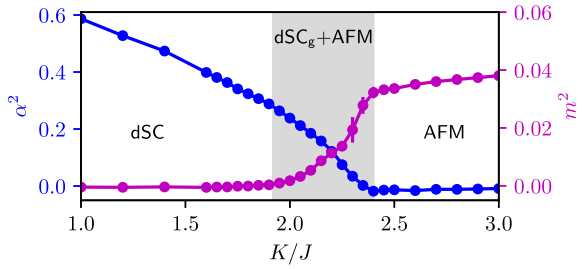

FIG. 2. QMC Phase diagram of our model at $V/t = 0.5$ and $U/t = 4.0$. Here, α is the dSC order parameter, m is the AFM order parameter.

$m \neq 0$, and therefore this is the $d\mathrm{SC}_g + \mathrm{AFM}$ phase. For $K/J > 2.40(5)$, we enter the pure AFM phase where only $m \neq 0$.

The phase diagram is also consistent with the results for the single-particle gap as well as the spin gap, see Figs. 3(b)–3(d). As shown in Fig. 3(c), in the nodal dSC region $K/J < 1.92(5)$, we have nodes at the K points, while the antinodal points X are gapped. The single-particle gaps open both in the $d\mathrm{SC}_g + \mathrm{AFM}$ and the AFM regions. Similarly, the gap to spinful excitations remains zero at Γ and M points in the $d\mathrm{SC}_g + \mathrm{AFM}$ and the AFM regions, due to the Goldstone modes resulting from the spin-rotation symmetry breaking.

Phase transitions.—The transitions from the dSC to the $d\mathrm{SC}_g + \mathrm{AFM}$ and from the $d\mathrm{SC}_g + \mathrm{AFM}$ to the AFM both appear to be continuous. The transition from the $d\mathrm{SC}_g + \mathrm{AFM}$ to the AFM is the conventional XY transition, and the data for the charge stiffness can be collapsed quite well with 3D XY exponents, see Figs. 4(a) and 4(b). The transition from the dSC to the $d\mathrm{SC}_g + \mathrm{AFM}$ is a more interesting one, which on theoretical ground we believe to be in the HGN class (see below). Using data collapse, we extract the critical exponents for this transition, as shown in Figs. 4(c) and 4(d). We estimate the correlation length exponent $\nu = 0.99(8)$ and the anomalous dimension of the AFM order-parameter $\eta_m = 0.55(2)$.

We also measured the Fermi velocity v_F, the dSC pairing velocity v_Δ defined via the nodal dispersion $E_g(\vec{q}') = \sqrt{v_F^2 q_x'^2 + v_\Delta^2 q_y'^2 + E_g^2(K)}$, and the spin-wave velocity v_s defined via the dispersion of Goldstone modes at the M point through $E_s(\vec{q}') = \sqrt{v_s^2 q'^2 + E_s^2(M)}$. To extract these velocities, we considered two different finite-size scaling schemes. In scheme 1, we fix $\delta q = 2\pi/L_{\max}$, and for system sizes less than $L_{\max} = 20$, $E_g(K + \vec{d}k_1)$, $E_g(K + \vec{d}k_2)$, and $E_s(\Gamma + \vec{d}k_1)$ are obtained by interpolation. After we obtain gap functions for each system size, we perform an $1/L$ extrapolation of the gap, and finally use the above formulas to obtain the velocities. In scheme 2, we first calculate the velocities based on the above formulas, and then perform the $1/L$ extrapolation of the velocities. The velocities obtained from these schemes are shown in Fig. 3(e). Although our data suffer from finite-size effects due to the curvature of the dispersion [43], we see a tendency for the velocity differences to decrease on approaching the transition from dSC to $d\mathrm{SC}_g + \mathrm{AFM}$. This is in line with the field theory prediction that at long distances, all three velocities become equal at this transition [50].

Low energy theory.—The transition from the nodal dSC to the $d\mathrm{SC}_g + \mathrm{AFM}$ is of particular interest since it hosts gapless nodal fermions. The corresponding low-energy theory was discussed in Ref. [50]. In the following we will show that it can be further mapped to the HGN theory. The nodal dSC phase has nodes located at $(\pm\pi/2, \pm\pi/2)$, as shown in Fig. 3. These four nodes can be divided into two pairs, forming two four-component Dirac fermions. At this transition, in addition to the nodal fermions, we also have gapless AFM modes $\vec{N}$, which couple linearly to the

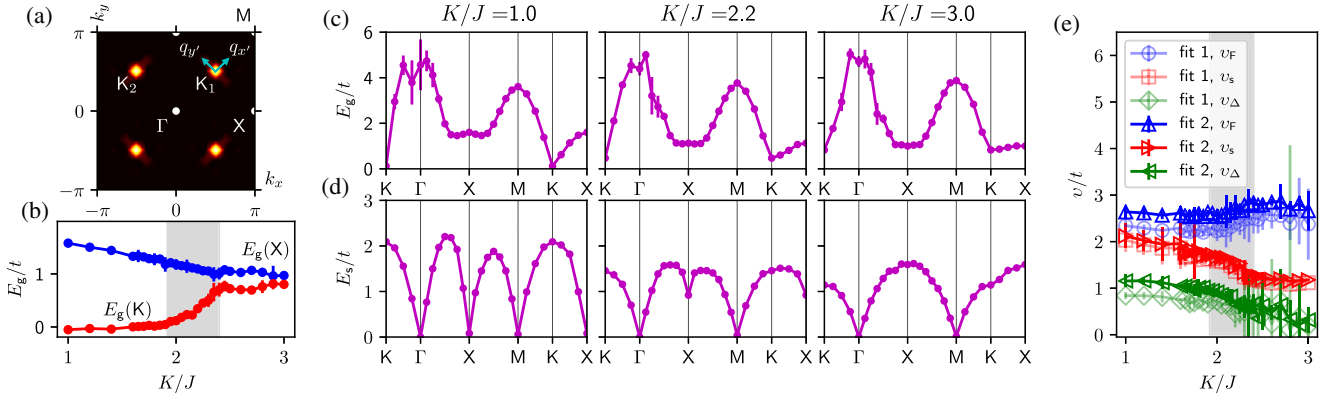

FIG. 3. Single-particle and spin gaps and velocities. (a) The first Brillouin zone (BZ) of the square lattice. Four light points are the location of nodes, and the lightness of the color denotes integrated spectral weight $A(\vec{k}, \omega)$ over a small energy window near the Fermi level $(0, 0.5t)$. (b) Single-particle gap at the nodal point (K) and the antinodal point (X) extrapolated to thermodynamic limit. (c) Single-particle gap along the path K-Γ-X-M-K-X of BZ at $L = 16$. (d) Spin gap along the same path of BZ at $L = 16$. (e) Fermi velocity, spin-wave velocity, and pairing velocity extracted using two different fitting schemes.

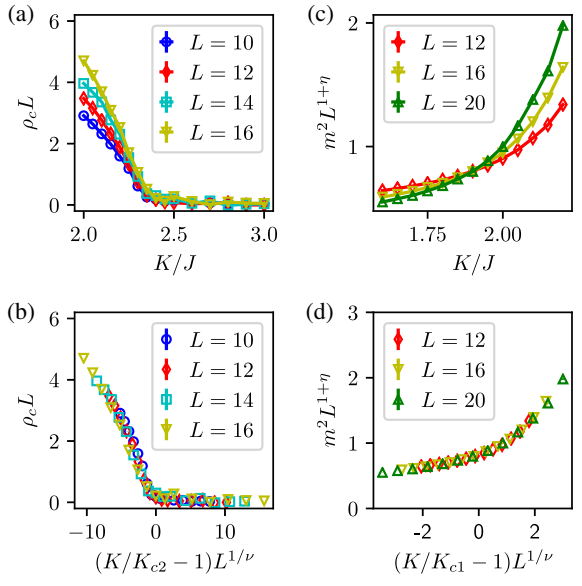

FIG. 4. Data collapse to obtain critical exponents. (a) Charge stiffness ρ_c for different system sizes near the second phase transition from the coexistence phase to the AFM phase. (b) Data collapse of the charge stiffness in (a) with $K_{c2} = 2.40(5)$ leads to $\nu \approx 0.67$. (c) Squared AFM order parameter m^2 near the transition from the nodal dSC phase to the coexistence phase. (d) Data collapse of m^2 in (c) with $K_{c1} = 1.92(5)$ leads to $\nu = 0.99(8)$ and $\eta = 0.55(2)$.

corresponding Dirac fermion bilinear. After a few basis transformations, while ignoring the difference between the three velocities v_F, v_Δ, v_s, and rescaling them to unity, one arrives at the following Lagrangian [50]:

$$\mathcal{L} = \bar{\Psi}\partial\!\!\!/\Psi + \frac{1}{2}(\partial_\mu \vec{N})^2 + u(\vec{N}^2)^2 + g\vec{N}\cdot(\Psi^\dagger \tau^y \vec{\sigma}\sigma^y \Psi^\dagger + \text{H.c.}), \tag{2}$$

where $\partial\!\!\!/ = \gamma^\mu \partial_\mu$, and the Pauli matrices $\vec{\tau}$ act in the particle-hole space of the original microscopic fermions c. The $4-\epsilon$ RG calculations predict that the difference between velocities eventually flows to zero, so that the above isotropic description is valid for a continuous transition. The isotropic free Dirac fermions have an O(8) symmetry, which can be made manifest by employing Majorana basis ($\Psi = \eta_1 + i\eta_2$). We will now exploit this O(8) symmetry to transform the critical theory into a well-known form. The coupling term in the Majorana basis becomes $g\vec{N}\cdot(\eta^T \tau^y \vec{\Sigma}\eta)$ with $\vec{\Sigma} = (\sigma^z\rho^x, \rho^z, -\sigma^x\rho^x)$, where the Pauli matrices $\rho^{x,y,z}$ act in the Majorana space (η_1, η_2). With an orthogonal transformation $\mathrm{O} = (i/\sqrt{2})(\sigma^y\rho^z - \rho^y) \in \mathrm{O}(8)$ of the free theory, the coupling can be transformed into $g\vec{N}\cdot(\eta'^T \tau^y \vec{\Sigma}'\eta')$ with $\eta' = \mathrm{O}\eta$ and $\vec{\Sigma}' = (\sigma^x, -\sigma^y\rho^y, \sigma^z)$, which if written in terms of complex fermions, is nothing but the standard HGN coupling $g\vec{N}\cdot(\Psi'^\dagger \tau^y \vec{\sigma}\Psi')$ where $\Psi' = \eta'_1 + i\eta'_2$. Therefore, the low-energy theory is equivalent to the HGN model, and the transition should also belong to the chiral Heisenberg universality class with two four-component Dirac fermions [51–61]. The above field theory arguments also apply to a recent numerical QMC study of mean-field Hamiltonian of dSC to AFM transition [62]. The charge U(1) symmetry is *explicitly* broken in their model, and therefore it does not support a phase where the superconductor results from spontaneous symmetry breaking, or an AFM phase which preserves charge U(1). However, HGN is still the correct effective description of the spin-SU(2) breaking *transition* seen in their model. This is because the charge-U(1) doesn't play an important role across this transition from RG perspective, and our above analysis applies. The absence of charge U(1) also implies that in contrast to our model, there will not be a finite-T Berezinskii-Kosterlitz-Thouless transition. Although the complexity of our model limits us to 20×20 system size, the critical exponents we found, namely $\nu \approx 0.99$ and $\eta_m \approx 0.55$, are consistent with works which study the same universality class up to 40×40 size [57,62]. The limited size also limits our ability to perform a more detailed analysis of finite size corrections. It is worth noting that the values of η_m reported in previous numerical works differ from each other considerably, and lie in a window ranging from 0.45 to 1.2, which likely signals strong finite-size corrections for this exponent even for larger system sizes.

Discussion and conclusion.—Very broadly, the structure of our model is in the similar spirit as Refs. [63–67], where a desired ordered phase is obtained by coupling the corresponding fermionic bilinear to a fluctuating bosonic field, and then tuning the kinetic energy of the boson to obtain an order-disorder quantum critical point. The novelty of our model is that it allows one to access a spontaneously symmetry broken nodal SC phase, and its competition with AFM, a scenario realized in a large class of materials [1–16,26–32], and especially pressure tuned SC to AFM transition in layered organic Mott insulators [17–25]. Although our Hamiltonian involves terms that are not conventional, owing to the usual notions of universality of low-energy effective theory, we expect aspects such as the nature of quantum criticality as well as the topology of the phase diagram to correctly capture more realistic Hamiltonians (which typically suffer from the sign problem), as long as the symmetries and the filling match with our model. At the same time, we do not attempt to provide insight into questions such as the shape of the phase boundaries, effects related to geometrical frustration, or even the underlying mechanism for superconductivity in the aforementioned materials.

The competition between d-wave superconductivity and AFM is also explored in Monte Carlo studies of various multiband models [68–73]. In contrast to our model, in Refs. [68–73], the pairing order parameter is in fact on site,

and the superconductivity is not nodal. We also note an interesting proposal for a model of competing AFM and nodal dSC phases, Ref. [74]. In this purely electronic model, the value of the d-wave order parameter obtained on the largest system size was rather small. and it might be interesting to revisit it.

Our model allows for adding orbital and Zeeman magnetic fields of arbitrary strength *without* introducing sign problem. It will be very interesting to study the destruction of dSC as either of these fields are ramped up. Another interesting question is to explore the possibility of destroying the dSC phase by proliferating *double* vortices, while keeping a single vortex gapped. This will lead to a fractionalized phase with topological order where nodal spinons are coupled to a Z_2 gauge field.

In summary, we constructed a sign-problem-free repulsive Hubbard model which hosts competing AFM and nodal d-wave phases. We found three different phases by tuning a single parameter K/J that controls the fluctuations of the bosonic fields: a nodal dSC phase at small K/J, an AFM phase at large K/J, and an intermediate phase with coexisting gapped d-wave and AFM orders. The phase transition between the coexistence phase and the AFM phase is a conventional 3D XY transition, while that between the coexistence phase and the nodal d wave also appears to be continuous, and belongs to the $2+1$-D HGN universality class.

We thank Fakher Assaad, John McGreevy for useful discussions, and Dan Arovas, Rafael Fernandes for comments on the draft. T. G. acknowledges support by the National Science Foundation under Grant No. DMR-1752417, and by an Alfred P. Sloan Research Fellowship. This work used the Extreme Science and Engineering Discovery Environment (XSEDE) [75], which is supported by National Science Foundation Grant No. ACI-1548562.

Note added.—Recently, we became aware of an article [62], which studies a *mean-field* Hamiltonian of nodal dSC with repulsive Hubbard-U. The relation to this work is discussed above in the section on low energy theory.

[1] M. R. Norman, Science **332**, 196 (2011).
[2] E. Dagotto, Rev. Mod. Phys. **66**, 763 (1994).
[3] P. A. Lee, N. Nagaosa, and X.-G. Wen, Rev. Mod. Phys. **78**, 17 (2006).
[4] F. Steglich, C. Bredl, W. Lieke, U. Rauchschwalbe, and G. Sparn, Physica B+C (Amsterdam) **126**, 82 (1984).
[5] G. R. Stewart, Rev. Mod. Phys. **56**, 755 (1984).
[6] A. Amato, Rev. Mod. Phys. **69**, 1119 (1997).
[7] C. Pfleiderer, Rev. Mod. Phys. **81**, 1551 (2009).
[8] P. G. Pagliuso, C. Petrovic, R. Movshovich, D. Hall, M. F. Hundley, J. L. Sarrao, J. D. Thompson, and Z. Fisk, Phys. Rev. B **64**, 100503(R) (2001).
[9] M. B. Maple, R. E. Baumbach, N. P. Butch, J. J. Hamlin, and M. Janoschek, J. Low Temp. Phys. **161**, 4 (2010).
[10] F. Steglich, J. Aarts, C. D. Bredl, W. Lieke, D. Meschede, W. Franz, and H. Schäfer, Phys. Rev. Lett. **43**, 1892 (1979).
[11] R. Joynt and L. Taillefer, Rev. Mod. Phys. **74**, 235 (2002).
[12] G. Knebel, M.-A. Méasson, B. Salce, D. Aoki, D. Braithwaite, J. P. Brison, and J. Flouquet, J. Phys. Condens. Matter **16**, 8905 (2004).
[13] T. Park, F. Ronning, H. Q. Yuan, M. B. Salamon, R. Movshovich, J. L. Sarrao, and J. D. Thompson, Nature (London) **440**, 65 (2006).
[14] H. Q. Yuan, F. M. Grosche, M. Deppe, C. Geibel, G. Sparn, and F. Steglich, Science **302**, 2104 (2003).
[15] T. Mito, S. Kawasaki, Y. Kawasaki, G. Q. Zheng, Y. Kitaoka, D. Aoki, Y.. Haga, and Y. Ōnuki, Phys. Rev. Lett. **90**, 077004 (2003).
[16] G. Aeppli, A. Goldman, G. Shirane, E. Bucher, and M.-C. Lux-Steiner, Phys. Rev. Lett. **58**, 808 (1987).
[17] F. Kagawa, K. Miyagawa, and K. Kanoda, Nature (London) **436**, 534 (2005).
[18] Y. Kurosaki, Y. Shimizu, K. Miyagawa, K. Kanoda, and G. Saito, Phys. Rev. Lett. **95**, 177001 (2005).
[19] S. Lefebvre, P. Wzietek, S. Brown, C. Bourbonnais, D. Jérome, C. Mézière, M. Fourmigué, and P. Batail, Phys. Rev. Lett. **85**, 5420 (2000).
[20] T. Arai, K. Ichimura, K. Nomura, S. Takasaki, J. Yamada, S. Nakatsuji, and H. Anzai, Phys. Rev. B **63**, 104518 (2001).
[21] S. Belin, K. Behnia, and A. Deluzet, Phys. Rev. Lett. **81**, 4728 (1998).
[22] S. M. De Soto, C. P. Slichter, A. M. Kini, H. H. Wang, U. Geiser, and J. M. Williams, Phys. Rev. B **52**, 10364 (1995).
[23] H. Mayaffre, P. Wzietek, D. Jérome, C. Lenoir, and P. Batail, Phys. Rev. Lett. **75**, 4122 (1995).
[24] K. Kanoda, K. Miyagawa, A. Kawamoto, and Y. Nakazawa, Phys. Rev. B **54**, 76 (1996).
[25] D. Jérome, Science **252**, 1509 (1991).
[26] G. R. Stewart, Rev. Mod. Phys. **83**, 1589 (2011).
[27] Q. Si, R. Yu, and E. Abrahams, Nat. Rev. Mater. **1**, 16017 (2016).
[28] P. Dai, Rev. Mod. Phys. **87**, 855 (2015).
[29] D. K. Pratt, W. Tian, A. Kreyssig, J. L. Zarestky, S. Nandi, N. Ni, S. L. Bud'ko, P. C. Canfield, A. I. Goldman, and R. J. McQueeney, Phys. Rev. Lett. **103**, 087001 (2009).
[30] S. Nandi, M. G. Kim, A. Kreyssig, R. M. Fernandes, D. K. Pratt, A. Thaler, N. Ni, S. L. Bud'ko, P. C. Canfield, J. Schmalian, R. J. McQueeney, and A. I. Goldman, Phys. Rev. Lett. **104**, 057006 (2010).
[31] D. Vollhardt and P. Wolfle, *The Superfluid Phases of Helium 3* (Taylor and Francis, London, 1990).
[32] L. Balents, C. R. Dean, D. K. Efetov, and A. F. Young, Nat. Phys. **16**, 725 (2020).
[33] P. W. Anderson, Science **235**, 1196 (1987).
[34] C. Wu and S.-C. Zhang, Phys. Rev. B **71**, 155115 (2005).
[35] M. Oshikawa, Phys. Rev. Lett. **84**, 1535 (2000).
[36] M. B. Hastings, Phys. Rev. B **69**, 104431 (2004).
[37] A. I. Lichtenstein and M. I. Katsnelson, Phys. Rev. B **62**, R9283 (2000).
[38] M. Jarrell, T. Maier, M. H. Hettler, and A. N. Tahvildarzadeh, Europhys. Lett. **56**, 563 (2001).
[39] D. Sénéchal, P.-L. Lavertu, M.-A. Marois, and A.-M. S. Tremblay, Phys. Rev. Lett. **94**, 156404 (2005).
[40] M. Capone and G. Kotliar, Phys. Rev. B **74**, 054513 (2006).

[41] A. H. Nevidomskyy, C. Scheiber, D. Sénéchal, and A.-M. S. Tremblay, Phys. Rev. B **77**, 064427 (2008).

[42] S. S. Kancharla, B. Kyung, D. Sénéchal, M. Civelli, M. Capone, G. Kotliar, and A.-M. S. Tremblay, Phys. Rev. B **77**, 184516 (2008).

[43] See Supplemental Material at http://link.aps.org/supplemental/10.1103/PhysRevLett.126.217002 for more details of the mean-field theory and the extended results of QMC simulations, which includes Refs. [44–46].

[44] F. F. Assaad, Phys. Rev. B **71**, 075103 (2005).

[45] J. M. J. van Leeuwen, M. S. L. du Croo de Jongh, and P. J. H. Denteneer, J. Phys. A **29**, 41 (1996).

[46] A. W. Sandvik, Phys. Rev. B **57**, 10287 (1998).

[47] R. Blankenbecler, D. J. Scalapino, and R. L. Sugar, Phys. Rev. D **24**, 2278 (1981).

[48] F. Assaad and H. Evertz, in *Computational Many-Particle Physics*, Lecture Notes in Physics Vol. 739, edited by H. Fehske, R. Schneider, and A. Weiße (Springer, Berlin, Heidelberg, 2008), pp. 277–356.

[49] J. E. Hirsch, Phys. Rev. B **28**, 4059 (1983).

[50] L. Balents, M. P. A. Fisher, and C. Nayak, Int. J. Mod. Phys. B **12**, 1033 (1998).

[51] B. Rosenstein, H.-L. Yu, and A. Kovner, Phys. Lett. B **314**, 381 (1993).

[52] I. F. Herbut, Phys. Rev. Lett. **97**, 146401 (2006).

[53] I. F. Herbut, V. Juričić, and B. Roy, Phys. Rev. B **79**, 085116 (2009).

[54] F. F. Assaad and I. F. Herbut, Phys. Rev. X **3**, 031010 (2013).

[55] L. Janssen and I. F. Herbut, Phys. Rev. B **89**, 205403 (2014).

[56] F. P. Toldin, M. Hohenadler, F. F. Assaad, and I. F. Herbut, Phys. Rev. B **91**, 165108 (2015).

[57] Y. Otsuka, S. Yunoki, and S. Sorella, Phys. Rev. X **6**, 011029 (2016).

[58] N. Zerf, L. N. Mihaila, P. Marquard, I. F. Herbut, and M. M. Scherer, Phys. Rev. D **96**, 096010 (2017).

[59] J. A. Gracey, Phys. Rev. D **97**, 105009 (2018).

[60] P. Buividovich, D. Smith, M. Ulybyshev, and L. von Smekal, Phys. Rev. B **98**, 235129 (2018).

[61] T. C. Lang and A. M. Läuchli, Phys. Rev. Lett. **123**, 137602 (2019).

[62] Y. Otsuka, K. Seki, S. Sorella, and S. Yunoki, Phys. Rev. B **102**, 235105 (2020).

[63] E. Berg, M. A. Metlitski, and S. Sachdev, Science **338**, 1606 (2012).

[64] Y. Schattner, S. Lederer, S. A. Kivelson, and E. Berg, Phys. Rev. X **6**, 031028 (2016).

[65] E. Berg, S. Lederer, Y. Schattner, and S. Trebst, Annu. Rev. Condens. Matter Phys. **10**, 63 (2019).

[66] X. Y. Xu, Z. H. Liu, G. Pan, Y. Qi, K. Sun, and Z. Y. Meng, J. Phys. Condens. Matter **31**, 463001 (2019).

[67] Z.-X. Li and H. Yao, Annu. Rev. Condens. Matter Phys. **10**, 337 (2019).

[68] Y. Schattner, M. H. Gerlach, S. Trebst, and E. Berg, Phys. Rev. Lett. **117**, 097002 (2016).

[69] P. T. Dumitrescu, M. Serbyn, R. T. Scalettar, and A. Vishwanath, Phys. Rev. B **94**, 155127 (2016).

[70] Z.-X. Li, F. Wang, H. Yao, and D.-H. Lee, Phys. Rev. B **95**, 214505 (2017).

[71] S. Lederer, Y. Schattner, E. Berg, and S. A. Kivelson, Proc. Natl. Acad. Sci. U.S.A. **114**, 4905 (2017).

[72] X. Wang, Y. Schattner, E. Berg, and R. M. Fernandes, Phys. Rev. B **95**, 174520 (2017).

[73] M. H. Christensen, X. Wang, Y. Schattner, E. Berg, and R. M. Fernandes, Phys. Rev. Lett. **125**, 247001 (2020).

[74] F. F. Assaad, M. Imada, and D. J. Scalapino, Phys. Rev. Lett. **77**, 4592 (1996).

[75] J. Towns, T. Cockerill, M. Dahan, I. Foster, K. Gaither, A. Grimshaw, V. Hazlewood, S. Lathrop, D. Lifka, G. D. Peterson, R. Roskies, J. Scott, and N. Wilkins-Diehr, Comput. Sci. Eng. **16**, 62 (2014).